Optics & Laser Technology 47 (2013) 64–71

Contents lists available at SciVerse ScienceDirect

Optics & Laser Technology

journal homepage: www.elsevier.com/locate/optlastec

Defect detection for tire laser shearography image using curvelet transform based edge detector

Yan Zhang *, Tao Li, Qingling Li

College of Electromechanical Engineering, Qingdao University of Science and Technology, 99 Songling Road, Qingdao 266061, China

ARTICLE INFO

Article history:
Received 4 July 2012
Received in revised form
13 August 2012
Accepted 20 August 2012
Available online 12 October 2012

Keywords:
Tire shearography image
Curvelet transform
Canny operator

ABSTRACT

In this work, we approach the analysis and segmentation of tire laser shearography image by combining curvelet transform and Canny edge detection to detect defects in tire surface. We rely on the feature of curvelet that edge features can be represented with larger coefficients in sub-highest frequency band thus we modify curvelet coefficients to enhance image edges before further edge detection operations. Only the most important coefficients that contribute to rebuild edges are selected to reconstruct the image while most small coefficients are cut off. This would result in a reconstructed image more convenient for edge detection and the time complexity is reduced on the other hand. Furthermore, the eight-neighborhood bilinear interpolation non-maximum suppression method is introduced to improve the performance of Canny edge detection. Our detection results are evaluated on test laser shearography images using the proposed scheme and compare favorably to the state-of-the-art methods.

1. Introduction

Edges hold much information about signals [1]. In computer vision and image processing, edge detection concerns the localization of significant variations of the gray level image and the identification of the physical phenomena that originated them. The reason for this is that edges form the outline of an object which means that if the edges in an image are detected accurately, all of the objects can be located and basic properties can be measured. In the past few years, there has been significant interest in edge detection approaches which has been widely used in many applications such as medical image, computer vision, and robotics depends in many cases on the results of edge detection. It is difficult to design a general edge detection algorithm which performs well in many contexts and captures the requirements of subsequent processing stages. Consequently, over the history of digital image processing a variety of edge detectors have been devised which differ in their mathematical and algorithmic properties. Many different edge detectors such as the Sobel operator, the LoG operator and the Canny detector were presented in early days [2–4]. Recently, based on the techniques that include geometry, statistics, wavelet, and neural theory, some new edge detectors were derived [5–8]. The regularization or smoothing [9] and optimal approaches of Canny [10] have led to several efficient continuous operators for noisy and blurred images [11–15]. Also, three different soft computing approaches to edge detection for image segmentation are most frequently used. These are (1) Fuzzy based approach [16], (2) Genetic Algorithm based approach [17] and (3) Neural Network based approach [18].

Laser shearography images generated from tire defection experiments are often unavoidably interfered with much high frequency speckle noise which greatly increases the difficulty in defects detection in tire laser shearography image. The motive of edge detection for tire laser shearography image is to extract speckle fringes therefore tire defects are detected thereafter.

In this paper, we propose a curvelet based improved Canny edge detection scheme to detect edges of defection in tire laser shearography images. The proposed method utilizes the feature of curvelet transform whose edge information can be represented with the larger coefficients in the high frequency band. Larger curvelet coefficients corresponding to edge information are selected through thresholding and modified by a function, therefore, to enhance image edges before further edge detection operations. The proposed scheme is efficient filtering high frequency speckle noise and preserving edge information simultaneously which highly overcomes the disadvantage and contradiction of noise suppression and edge maintenance. An eight-neighborhood bilinear interpolation non-maximum suppression method which outperforms the eight-neighborhood gradient value method is introduced to increase edge detection accuracy.

In the following sections, we discuss the advantages of curvelet transform in presenting image edge information. We probe into the shortcomings of conventional edge detection methods.

* Corresponding author.
E-mail addresses: zy@qust.edu.cn, a.zh@aol.com (Y. Zhang), litao@qust.edu.cn (T. Li), liqingling@qust.edu.cn (Q. Li).

0030-3992/$ - see front matter © 2012 Elsevier Ltd. All rights reserved.
http://dx.doi.org/10.1016/j.optlastec.2012.08.023

In Section 4, we introduce our proposed curvelet based edge detection method for tire laser shearography image and furthermore, the superiority of the eight-neighborhood bilinear interpolation non-maximum suppression method demonstrated. We give the experimental results in Section 5. Finally, we discuss the experimental results of the proposed algorithm and conclude the paper.

2. Curvelet transform

Motivated by the need of image analysis, Candes and Donoho first proposed curvelet transform [19]. Unlike the wavelet transform, which fails to represent objects containing randomly oriented edges and curves as it is not good at representing line singularities, the curvelet transform, as a higher dimensional generalization of the wavelet transform designed to represent images at different scales and different angles, is able to catch the edge singularities efficiently with very few coefficients in a non-adaptive manner. Fig. 1 shows the edge representation by wavelets and curvelets.

Second generation curvelet transform has two different digital implementations [20]. The first digital transformation is based on unequally-spaced fast Fourier transforms (USFFT) while the second is based on the wrapping of specially selected Fourier samples. These new discrete curvelet transforms are simpler, faster and less redundant compared to their first generation version. Curvelets via wrapping has been used for this work as this is the fastest curvelet transform currently available [21]. If $f[t_1, t_2]$, $0 \le t_1, t_2 < n$ is taken to be a Cartesian array and $\hat{f}[n_1,n_2]$ to denote its 2D Discrete Fourier Transform, then the architecture of curvelets via wrapping is as follows [20]:

1. 2D FFT (fast Fourier transform) is applied to obtain Fourier samples $\hat{f}[n_1,n_2]$.
2. For each scale j and angle l, the product $\tilde{U}_{j,l}[n_1,n_2]\hat{f}[n_1,n_2]$ is formed, where $\tilde{U}_{j,l}[n_1,n_2]$ is the discrete localizing window.

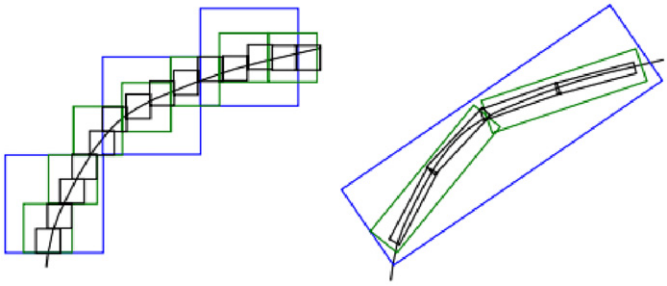

Fig. 1. Edge representation by wavelets (left) and curvelets (right).

3. This product is wrapped around the origin to obtain

$$\tilde{f}_{j,l}[n_1,n_2] = W(\tilde{U}_{j,l}\hat{f})[n_1,n_2] \quad (1)$$

where the range for n_1 and n_2 is now $0 \le n_1 < L_{1,j}$ and $0 \le n_2 < L_{2,j}$ (for θ in the range $(-\pi/4,\pi/4)$). We let $P_{j,l}$ be a parallelogram containing the support of the discrete localizing window $\tilde{U}_{j,l}[n_1,n_2]$. We suppose that at each scale j, there exists two constants $L_{1,j} \sim 2^j$ and $L_{2,j} \sim 2^{j/2}$ such that, for every orientation θ_l, one can tile the two-dimensional plane with translates of $P_{j,l}$ by multiples of $L_{1,j}$ in the horizontal direction and $L_{2,j}$ in the vertical direction. The corresponding periodization of the windowed data $d[n_1,n_2] = \tilde{U}_{j,l}[n_1,n_2]\hat{f}[n_1,n_2]$ reads

$$Wd[n_1,n_2] = \sum_{m_1 \in Z} \sum_{m_2 \in Z} d[n_1 + m_1 L_{1,j},\, n_2 + m_2 L_{2,j}] \quad (2)$$

4. Apply the inverse 2D FFT to each $\tilde{f}_{j,l}$, hence collecting the discrete coefficients $c^D(j,l,k)$.

Fig. 2 shows an example of image decomposition with curvelet. Fig. 2(a) is an original test image, Fig. 2(b) is the coefficients of curvelet transform and Fig. 2(c) is the partial reconstruction of original face image using 10% of coefficients.

The second generation curvelet transform is an effective frequency analysis for each subband being divided in the frequency domain. As higher the frequency, the larger the bandwidth of the subband becomes. For each subband, this is divided further into several regions with different polar angles. The curvelet coefficients under a certain scale can be obtained through the inverse Fourier transform of the corresponding regions.

In an image, the presence of an edge feature is usually accompanied by a drastic change of the pixels gray value. As a result, edge features often appear at the higher frequency band in the frequency domain. Curvelet is an edge based multi-scale representation of the image, with the edge information corresponding to larger curvelet coefficients. Consequently, the edge information can be represented with the larger coefficients in high frequency band. The highest band, however, usually corresponds to the frequency response of isolated points and noise; thus the frequency response of the edge features should be located at the sub-highest frequency band, see Fig. 3 [22].

3. Edge detection methods for tire laser shearography image

Edge detection is a fundamental tool in image processing and computer vision, particularly in the areas of feature detection and feature extraction, which aim at identifying points in a digital image at which the image brightness changes sharply or, more formally, has discontinuities. There are many methods for edge

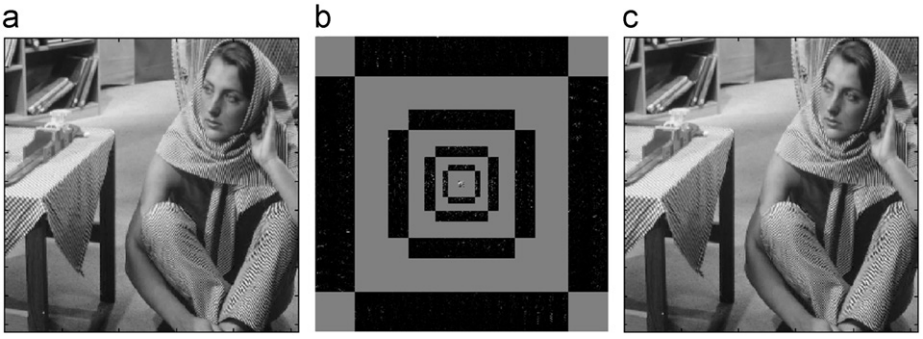

Fig. 2. Image decomposition with curvelet: (a) test barbara image, (b) the coefficients of curvelet transform, and (c) the partial reconstruction of original face image (10% of coefficients).

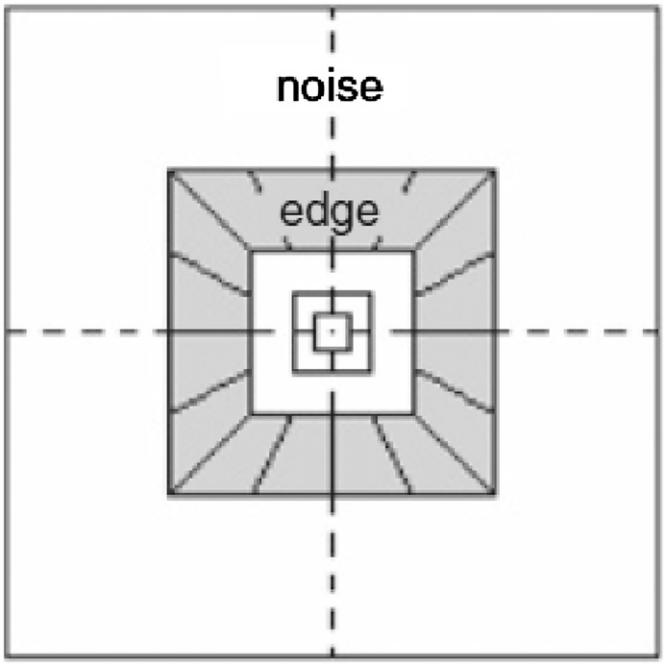

Fig. 3. Curvelet subband partition in frequency domain.

detection, but most of them can be grouped into two categories, search-based and zero-crossing based. The search-based methods detect edges by first computing a measure of edge strength, usually a first-order derivative expression such as the gradient magnitude, and then searching for local directional maxima of the gradient magnitude using a computed estimate of the local orientation of the edge, usually the gradient direction. The zero-crossing based methods search for zero crossings in a second-order derivative expression computed from the image in order to find edges, usually the zero-crossings of the Laplacian or the zero-crossings of a non-linear differential expression. A survey of a number of different edge detection methods can be found in Ref. [23].

3.1. Sobel operator

Sobel operator is one of the gradient operators that are widely used in many applications. The operator calculates the gradient of the image intensity at each point, giving the direction of the largest possible increase from light to dark and the rate of change in that direction.

Fig. 4(b) shows test results of tire shearography image using the Sobel operator from which we can see that even though the Sobel operator can smooth noise it also detects fake edges.

3.2. LoG operator

One of the first and also most common edge detectors is based on the Laplacian of the Gaussian (LoG). Given an input image $f(x,y)$, this image is convolved by a Gaussian kernel

$$g(x,y,t)=\frac{1}{2\pi t}e^{-(x^2+y^2)/(2t)} \tag{3}$$

at a certain scale t to give a scale-space representation $L(x,y,t)=g(x,y,t)\times f(x,y)$. Then, the Laplacian operator $\nabla^2 L=L_{xx}+L_{yy}$ is computed, which usually results in strong positive responses for dark blobs of extent $\sqrt{2t}$ and strong negative responses for bright blobs of similar size.

Fig. 4 shows test results of tire shearography image with interference fringe using conventional edge detection operators. We test tire shearography image using different values σ. σ is the standard deviation used in smoothing function which determine how fuzzy the image is after smoothing. The experimental results show that more speckle noise is suppressed with bigger σ values (as can be seen in Fig. 4(e) in which $\sigma=3.5$) and less fake edges are generated. However, the discontinuity of edge becomes severe when σ value increases. This brings difficulty for detecting tire defects because useful edge information of defects is also incomplete.

3.3. Canny edge detection algorithm

Although John Canny's work was done in the early days of computer vision, the Canny edge detector (including its variations) is still a state-of-the-art edge detector [24]. Unless the preconditions are particularly suitable, it is difficult to find an edge detector that performs significantly better than the Canny edge detector. The Canny edge detector uses a filter based on the first derivative of a Gaussian, because it is susceptible to noise present on raw unprocessed image data, so to begin with, the raw image is convolved with a Gaussian filter:

$$M(x,y)=G(x,y,\sigma)f(x,y) \tag{4}$$

where $f(x,y)$ is the original image and $G(x,y,\sigma)$ is the Gaussian smoothing operator. An edge in an image may point in a variety of directions, so the Canny algorithm uses four filters to detect horizontal, vertical and diagonal edges in the blurred image when finding the intensity gradient of the image:

$$S(x,y)=\sqrt{P^2(x,y)+Q^2(x,y)} \tag{5}$$

$$\theta(x,y)=\arctan\left|Q(x,y)/P(x,y)\right| \tag{6}$$

where

$$P(x,y)\approx[M(x,y+1)-M(x,y)+M(x+1,y+1)-M(x+1,y)]/2 \tag{7}$$

$$Q(x,y)\approx[M(x,y)-M(x+1,y)+M(x,y+1)-M(x+1,y+1)]/2 \tag{8}$$

Given estimates of the image gradients, a search is then carried out to determine if the gradient magnitude assumes a local maximum in the gradient direction. Non-maximum suppression is used to make sure $S(x,y)=0$ if it is less than the maximum so that the width of detected edge is one pixel. Double thresholds are used and the larger threshold is decided by using the Ostu method [26]. Once this process is complete we have a binary image where each pixel is marked as either an edge pixel or a non-edge pixel. From complementary output from the edge tracing step, the binary edge map obtained in this way can also be treated as a set of edge curves, which after further processing can be represented as polygons in the image domain.

The Canny edge detection method has two disadvantages. The Gaussian filter is used to smooth the image. The scheme has a high location precision but weak smoothness and noise restraint ability with a smaller σ, such as $\sigma=0.3$ see Fig. 4(h). With a bigger σ, $\sigma=2$ for example, however, the filter size increases which would increase computation and cause edge shifting seriously as can be see in Fig. 4(g). On the other hand, the use of non-maximum suppression affects the accuracy of edge detection which causes the disconnection of edge points.

Those three methods mentioned above depend on first order or second order differentiation to compute the change in intensity, their properties differ as they inhabit different differentiation operators or smoothing stages. Moreover, intensity gradient might amplify high frequency components (noise) and distort the original edges of the image being detected since abrupt

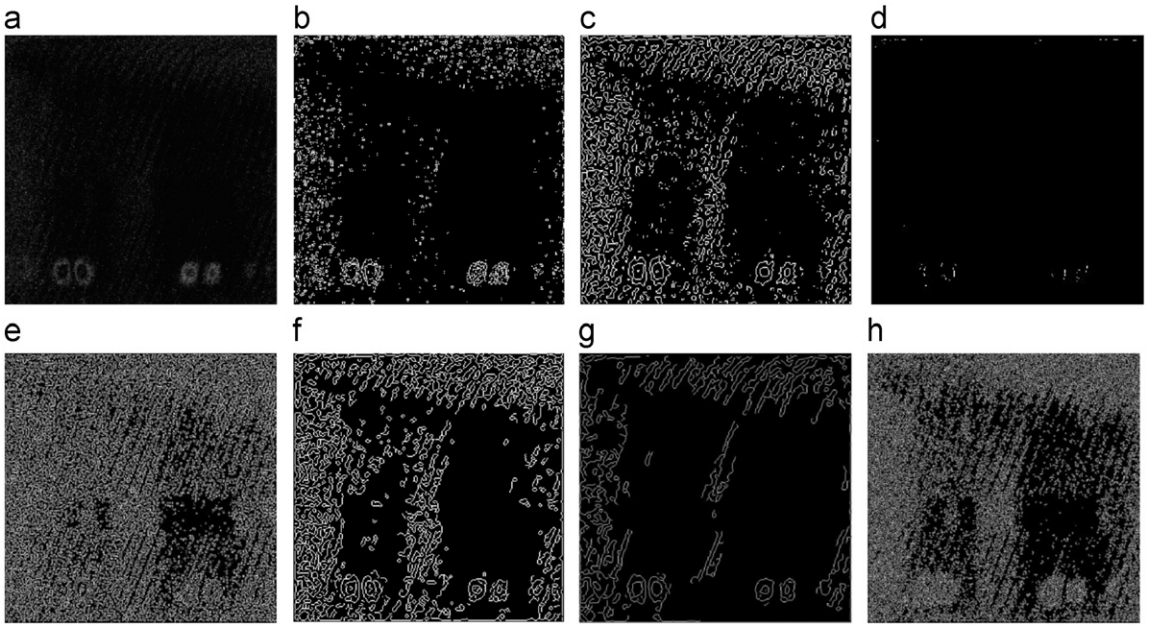

Fig. 4. Edge detection results based on conventional edge detection operators: (a) tire shearography image with interference fringe, (b) edge detection using the default Sobel operator, (c) edge detection using default LoG operator, (d) edge detection using LoG operator with $\sigma=3.5$, (e) edge detection using LoG operator with $\sigma=1.5$, (f) edge detection using default Canny operator, (g) edge detection using Canny operator with $\sigma=2.0$, and (h) edge detection using Canny operator with $\sigma=3.5$.

changes in image intensity may correspond to different forms of noise, see experimental results in Fig. 4. Filters are used to smoothing images however, that would lead to details loss.

4. Edge detection using curvelet transform and Canny operator

The curvelet transform performs well in representing images containing edges; therefore, we can use it to enhance image edges before further edge detection operations. This can be achieved by modifying curvelet coefficients which are modified by a function. This function however gives rise to the drawback amplifying the noise (linearly) as well as the signal of interest. We introduce explicitly the noise standard deviation σ in the equation. The coefficients are multiplied by y_c, where y_c is defined by [25]

$$
\begin{aligned}
&y_c(x,y)=1 \quad \text{if } x<c\sigma\\
&y_c(x,y)=\frac{x-c\sigma}{c\sigma}\left(\frac{m}{c\sigma}\right)^p+\frac{2c\sigma-x}{c\sigma} \quad \text{if } c\sigma<x<2c\sigma\\
&y_c(x,\sigma)=\left(\frac{m}{x}\right)^p \quad \text{if } 2c\sigma\le x<m\\
&y_c(x,\sigma)=\left(\frac{m}{x}\right)^s \quad \text{if } x\ge m
\end{aligned}
\tag{9}
$$

Here, degree of nonlinearity is determined by p and dynamic range compression is introduced by s. Using a nonzero s will enhance the faintest edges and soften the strongest edges at the same time. c Becomes a normalization parameter, and a c value larger than three guaranties that the noise will not be amplified. The m parameter is the value under which coefficients are amplified. This value depends obviously on the pixel values inside the curvelet scale. Therefore, we found it necessary to derive the m value from the data. Two options are possible [25]:

- m can be derived from the noise standard deviation ($m=K_m\sigma$) using an additional parameter K_m. The advantage is that K_m is now independent of the curvelet coefficient values, and therefore much easier for a user to set.
- m can also be derived from the maximum curvelet coefficient M_c of the relative band ($m=lM_c$, with $l<1$). In this case, choosing for instance $c=3$ and $l=0.5$, we amplify all coefficients with an absolute value between 3σ and half the maximum absolute value of the band.

When coefficients are amplified we reconstruct the enhanced image from the modified curvelet coefficients. For the reasons we mentioned in Section 2, in the proposed method we first sort the coefficients for the higher frequency bands and then select, for the magnitude, the top 1% in our experiment for reconstructing the image. According to our experiments, we can obtain satisfactory results even with less than top 1% coefficients. Here we choose the top 1% for the balance between experimental results and the time complexity of algorithm which would not effect experimental results at all. Thereafter, filter the reconstructed image using Gaussian filter (with $\sigma=4$).

Gradient is computed and then the eight-neighborhood bilinear interpolation non-maximum suppression (NMS) method is performed, see Fig. 5.

The thresholding with hysteresis uses a hysteresis loop to provide a more connected result. Any pixel above the upper threshold is turned white. The surround pixels are then searched recursively. If the values are greater than the lower threshold they are also turned white. The result is that there are many fewer specks of white in the resulting image.

In performing the improved non-maximum suppression method, we divided the pixel's eight neighborhoods into four quadrants according to its gradient angle $\theta(i,j)$, $-90^\circ\le\theta(i,j)\le 90^\circ$ and verdict if the pixel's gradient value is maximum or not along the direction of the pixel's gradient according to interpolation result. That is to say, when $-90^\circ\le\theta(i,j)\le 0^\circ$, we utilize the pixel's neighborhoods' in the second and fourth quadrants to perform bilinear interpolation in both horizontal and vertical direction to compare. Otherwise, when

$0^\circ \le \theta(i,j) \le 90^\circ$, we utilize the pixel's neighborhoods' in the first and third quadrants to perform bilinear interpolation in both horizontal and vertical direction to compare.

a) When $0^\circ \le \theta(i,j) \le 90^\circ$:
Horizontal interpolation in the first quadrant

$$\begin{cases} u_1 = S(x-1,y)+\cos[\theta(x,y)][S(x-1,y+1)-S(x-1,y)] \\ l_1 = S(x,y)+\cos[\theta(x,y)][S(x,y+1)-S(x,y)] \end{cases} \quad (10)$$

Vertical direction bilinear interpolation:

$$v_1 = u_1+\sin[\theta(x,y)](l_1-u_1) \quad (11)$$

Horizontal interpolation in the third quadrant:

$$\begin{cases} u_2 = S(x,y-1)+\cos[\theta(x,y)][S(x,y)-S(x,y-1)] \\ l_2 = S(x+1,y-1)+\cos[\theta(x,y)][S(x+1,y)-S(x+1,y-1)] \end{cases} \quad (12)$$

Vertical direction bilinear interpolation

$$v_2 = u_2+\sin[\theta(x,y)](l_2-u_2) \quad (13)$$

If $S(x,y) \ge v_1$ and $S(x,y) \ge v_2$, then $S(x,y)$is maximum; else $S(x,y)$ is not maximum.

b) When $-90^\circ \le \theta(i,j) \le 0^\circ$:
Horizontal interpolation in the second quadrant

$$\begin{cases} u_3 = S(x-1,y-1)+\cos[\theta(x,y)][S(x-1,y)-S(x-1,y-1)] \\ l_3 = S(x,y)+\cos[\theta(x,y)][S(x,y)-S(x,y-1)] \end{cases} \quad (14)$$

Vertical direction bilinear interpolation

$$v_3 = u_3+\sin[\theta(x,y)](l_3-u_3) \quad (15)$$

Horizontal interpolation in the fourth quadrant:

$$\begin{cases} u_4 = S(x,y)+\cos[\theta(x,y)][S(x,y+1)-S(x,y)] \\ l_4 = S(x+1,y)+\cos[\theta(x,y)][S(x+1,y+1)-S(x+1,y)] \end{cases} \quad (16)$$

Vertical direction bilinear interpolation:

$$v_4 = u_4+\sin[\theta(x,y)](l_4-u_4) \quad (17)$$

If $S(x,y) \ge v_3$ and $S(x,y) \ge v_4$, then $S(x,y)$ is maximum; else $S(x,y)$ is not maximum.

The horizontal interpolation and vertical direction bilinear interpolation of the pixel increase the accuracy of locating the edge in our improved non-maximum suppression method. Finally, double thresholds are used and the larger threshold is decided by using the Ostu method [26].

5. Experimental results

In our experiment, we test on tire laser shearography image with bubble defects to validate the proposed scheme. The Sobel operator, LoG operator and Canny edge detection algorithms are employed for comparison. There are several parameters in

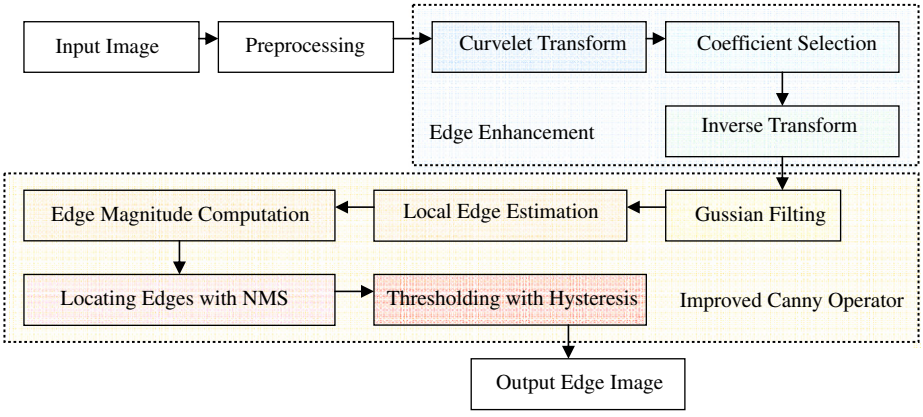

Fig. 5. Flowchart of the proposed method.

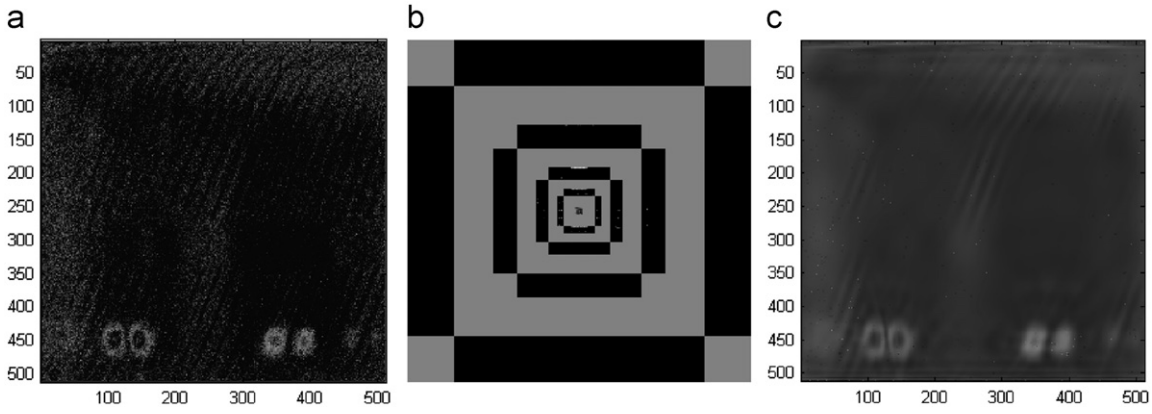

Fig. 6. Image decomposition with curvelet transform: (a) tire shearography image, (b) the coefficients of curvelet transform, and (c) the partial reconstruction of original shearography image (1% of coefficients).

Canny edge detection such as FILTER_SIZE=10, SIGMA=4, LOW_THRESHOLD_FACTOR=0.1 and HIGH_THRESHOLD_FACTOR=0.3. Also two parameters are taken in LOG scheme, the standard deviation σ_g of the Gaussian function and the threshold t to suppress false edges. In the proposed scheme, we first transform the laser shearography image into curvelet domain after preprocessing. We perform curvelet transform via the wrapping based method which may be simpler to understand and implement. Edge information which is represented by the larger coefficients in the high frequency band is selected to enhance edges. Fig. 6 shows a 512×512 tire laser shearography image, we transform the image into curvelet domain and select 1% of coefficients in partial reconstruction. As can be seen, the edges on the defects of tire are clearly visible in the reconstructed image and most of noises are eliminated as well.

Fig. 7 shows experimental results on tire shearography image to detect interference fringe of tire defects. Fig. 7(b) shows the partial reconstruction of test image using 0.1% of coefficients. We set the small coefficients that are smaller than our experiential threshold to zero. Here the threshold is 15. Fig. 7(c) shows the filtered (b) with Gaussian filter (with $\sigma=4$). The gradient

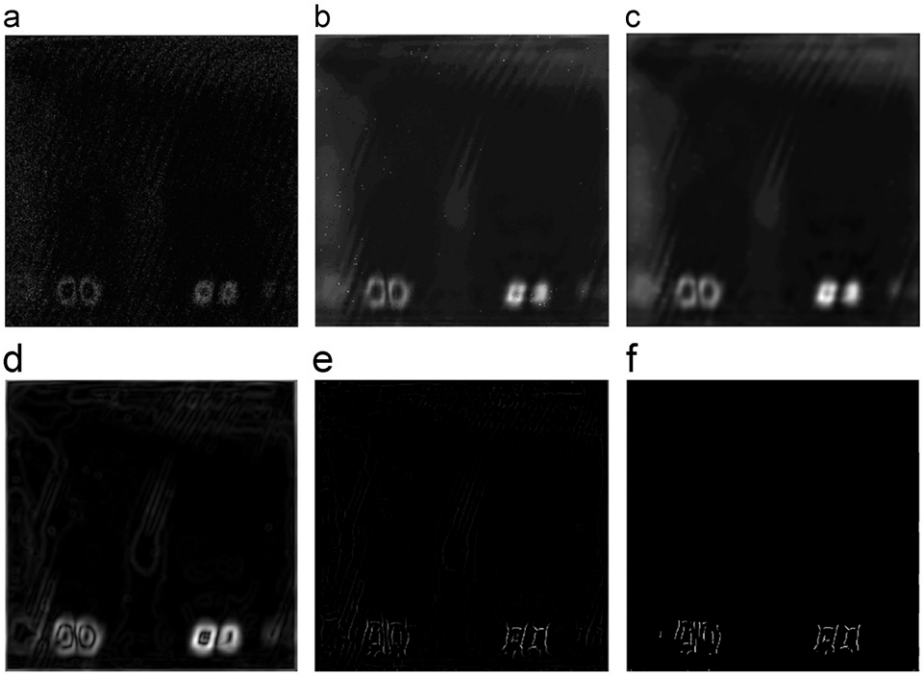

Fig. 7. Experiment on tire shearography image to detect interference fringe of tire defects: (a) test tire shearography image, (b) the partial reconstruction of test image (1% of coefficients), (c) filtered (b) with Gaussian filter (with $\sigma=4$), (d) the gradient magnitude of (c), (e) locate the edges with non-maximal suppression, and (f) thresholding (e) to eliminate.

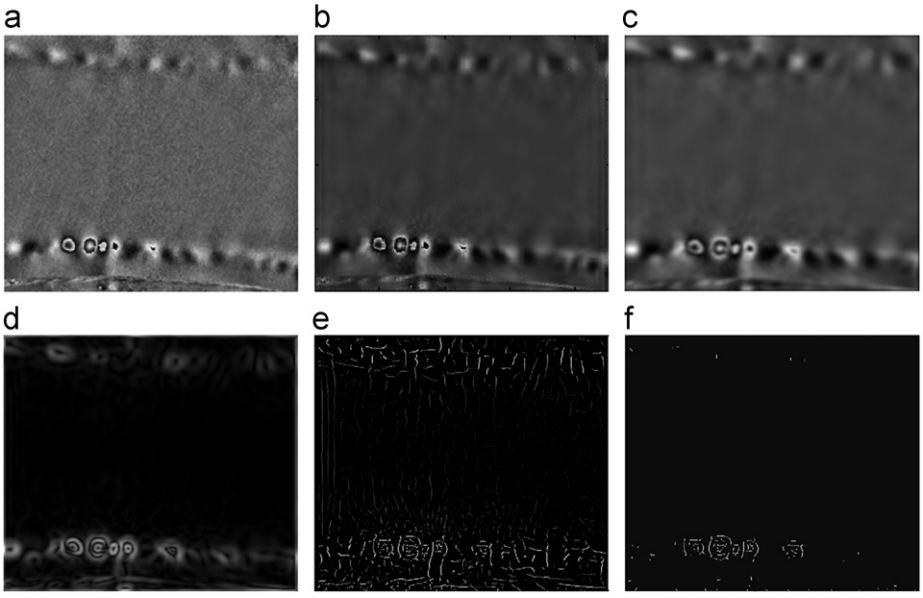

Fig. 8. Another experiment on tire shearography image to detect interference fringe of tire defects: (a)test tire shearography image, (b) the partial reconstruction of test image (1% of coefficients), (c) filtered (b) with Gaussian filter (with $\sigma=4$), (d) the gradient magnitude of (c), (e) locate the edges with non-maximal suppression, and (f) thresholding (e) to eliminate spurious responses.

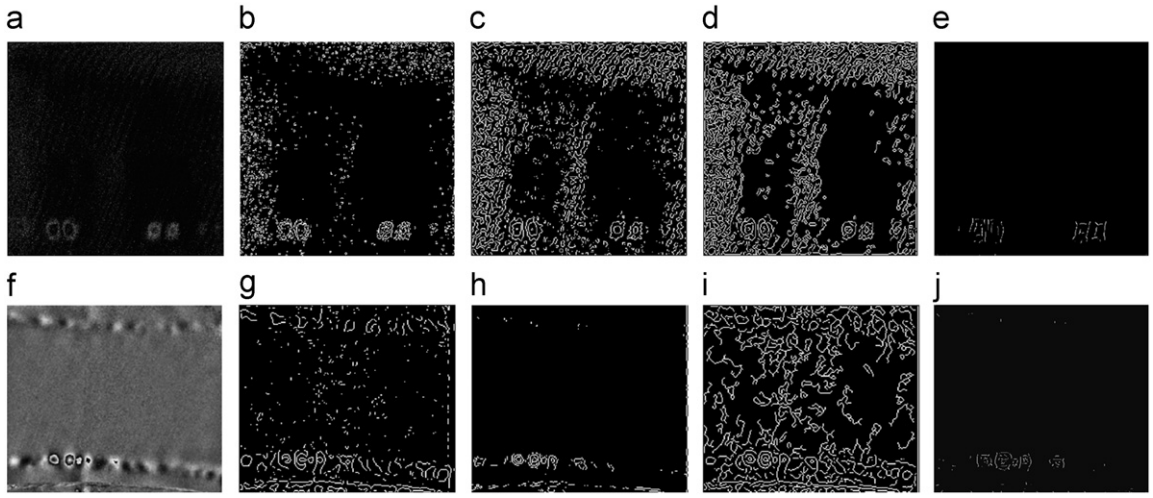

Fig. 9. Comparison of experimental results between the conventional edge detection methods and the proposed method: (a and f) test tire shearography image, (b and g) edge detection using default Sobel operator, (c and h) edge detection using default LoG operator, (d and i) edge detection using default Canny operator, (e and j) edge detection using our method.

magnitude of (c) is given in Fig. 7(d) and the edges are located with non-maximal suppression as can be seen in Fig. 7(e).

Finally, we threshold (e) to eliminate spurious responses. It can be seen in Fig. 7(f) that the tire defects in the tested laser shearography image are detected and located perfectly. There are spurious edges in Fig. 7(f) even after thresholding; however, these edge contours are usually harmless, and even if they are not removed by thresholding, they will be discarded by our subsequent algorithm since they contain no major edges.

Fig. 8 is the experiments on another tire shearography image. The presented scheme also achieves satisfying performances. The edges of defects are detected and located successfully and the false edges are eliminated at the same time.

An experimental comparison of the conventional default Sobel operator, LoG operator, Canny methods and the proposed method is given in Fig. 9. Edges obtained by Sobel operator, LoG operator and Canny edge detector are shown in Fig. 9(b, g), (c, h) and (d, i) respectively. Although an overwhelming majority of the correct edges are detected by these schemes, a large number of false edges are detected either, making it impossible to detect edges of defects. The proposed method successfully detects the defected edges and restrains fake edges effectively. Moreover, the use of eight-neighborhood bilinear interpolation non-maximum suppression method helps to improve the accuracy of location and connectivity outperforms the existing methods.

6. Conclusions

Edge contours representing object boundaries play a major role in object detection and recognition. The Canny edge detection method is still preferred in many real life applications since it produces single pixel thick, continuous edges. We tested three conventional edge detection methods: Canny, Sobel and LoG schemes. As demonstrated through a simple example in Fig. 4, locally maximum intensity changes along the gradient direction in a Gaussian-smoothed image do not pick up all the obvious edges in an image and a large number of false edges are detected which make it even worse in the application of tire defection detection in tire laser shearography images.

This paper mainly focuses on the study of edge detection for tire laser shearography image. We discuss the previously existing edge detection methods and demonstrate the superiority of the propose curvelet transform based improved Canny operator edge detection method. Experimental results indicate that our method outperforms the conventional Canny, Sobel and LoG edge detection methods in detecting accuracy of the edge of interference fringe. How to make better edge detector with application to tire laser shearography images which contain different defect patterns is an interesting problem to be solved.

References

[1] Wang X. Laplacian operator-based edge detectors. IEEE Transactions on Pattern Analysis and Machine Intelligence 2007;29(5):886–90.
[2] Pingle KK. Visual perception by a computer. In: Grasselli A, editor. Automatic interpretation and classification of images. Academic Press; New York 1969.
[3] Marr D, Hildreth EC. Theory of edge detection. In: Proceedings of the royal society of London series B. vol. 207; 1980. p. 187–217.
[4] Canny J. A computational approach to edge detection. IEEE Transactions on Pattern Analysis and Machine Intelligence 1986;8(6):679–98.
[5] Caselles V, Kimmel R, Sapiro G. Minimal surfaces based object segmentation. IEEE Transactions on Pattern Analysis and Machine Intelligence 1997;19(4):394–7.
[6] Faghih F, Michael M. Combining special and scale-space techniques for edge detection to provide a spatially adaptive wavelet-based noise filtering algorithm. IEEE Transactions on Image Processing 2002;11:1062–71.
[7] Konishi S, Yulle AL, Coughlan JM, Zhu SC. Statistical edge detection: learning and evaluating edge cues. IEEE Transactions on Pattern Analysis and Machine Intelligence 2003;25(1):57–74.
[8] Suzuki K, Horiba I, Sugie N. Neural edge enhancer for supervised edge enhancement from noisy image. IEEE Transactions on Pattern Analysis and Machine Intelligence 2003;25(12):1582–96.
[9] Torre V, Poggio TA. On edge detection. IEEE Transactions on Pattern Analysis and Machine Intelligence 1986;8(2):147–63.
[10] Mcllhagga W. The canny edge detector revisited. International Journal of Computer Vision 2011;91(3):251–61.
[11] Ziou D. Line detection using optimal irr filter. Pattern Recognition 1991;24(6):465–78.
[12] Deriche R. Using canny's criteria to derive a recursively implemented optimal edge detector. International Journal of Computer Vision 1987;1(2):167–87.
[13] Bourennane E, Gouton P, Paindavoine M, Truchetet F. Generalization of canny-deriche filter for detection of noisy exponential edge. Signal Processing 2002;12(10):1317–28.
[14] Jacob M, Unser M. Design of steerable filters for feature detection using canny-like criteria. IEEE Transsctions on Pattern Analysis and Machine Intelligence 2004;26(8):1007–19.
[15] Boyer KL, Sarkar S. On the localization performance measure and optimal edge detection. IEEE Transactions on Pattern Analysis and Machine Intelligence 1994;16(1):106–10.
[16] Zadeh LA. Some reflections on soft computing, granular computing and their roles in the conception, design and utilization of information/intelligent systems. Soft Computing 1998;2:23–5.
[17] Wen XB, Zhang H, Jiang ZT. Multiscale unsupervised segmentation of sar imagery using the genetic algorithm. Sensors 2008;8:1704–11.

[18] Moreira J, Costa LDF. Neural-based color image segmentation and classification using self-organizing maps. In: Proceedings of the Anais do IX SIBGRAPI; 1996. p. 47–54.
[19] Candes EJ, Donoho DL. Curvelets—a surprisingly effective nonadaptive representation for objects with edges. In: Rabut C, Cohen A, Schumaker LL, editors. Curves and surfaces. Nashville, TN: Vanderbilt University Press; 2000.
[20] Candes EJ, Demanet L, Donoho DL, Ying L. Fast discrete curvelet transform. Multiscale Modeling and Simulation 2006;5(3):861–99.
[21] Zhang Y, Yu B, Gu Haiming. Face recognition using curvelet based two-dimension principle component analysis. International Journal of Pattern Recognition and Artificial Intelligence; http://dx.doi.org/10.1142/S0218001412560095, in press.
[22] Zhou GY, Cui Y, Chen YL, Yang J, Rashvand HF. SAR image edge detection using curvelet transform and duda operator. Electronics Letters 2010;46(2):167–8.
[23] Ziou D, Tabbone S. Edge detection techniques: an overview. International Journal of Pattern Recognition and Image Analysis 1998;8(4):537–59.
[24] Shapiro LG, Stockman GC. Computer vision. London etc.: Prentice-Hall; 2001.
[25] Starck J, Murtagh F, Candès EJ, Donoho DL. Gray and color image contrast enhancement by the curvelet transform. IEEE Transactions on Image Processing 2003;12(6):706–17.
[26] Otsu Nobuyuki. A threshold selection method from gray-level histograms. IEEE Transactions on Systems, Man, and Cybernetrics 1979;9(1):62–6.